Check for updates

Journal of Mass Spectrometry

WILEY

Journal of MASS SPECTROMETRY

RESEARCH ARTICLE OPEN ACCESS

High-Throughput Equine Plasma Profiling Using Laser-Assisted Rapid Evaporative Ionisation Mass Spectrometry

Adrienn Molnár[1,2] | Matevž Arko[3] | Kaja Troha[4] | András Marton[5,6] | Boglárka Tauber[7] | Aleš Iglič[8] | György Tibor Balogh[5,9,10] | Júlia Balog[11] | Matej Hočevar[12] | Vesna Kadunc Kos[13] | Saba Battelino[4,14] | Veronika Kralj-Iglič[3] | Gitta Schlosser[1]

[1]MTA-ELTE Lendület (Momentum) Ion Mobility Mass Spectrometry Research Group, Faculty of Science, Institute of Chemistry, ELTE Eötvös Loránd University, Budapest, Hungary | [2]Hevesy György PhD School of Chemistry, ELTE Eötvös Loránd University, Budapest, Hungary | [3]Laboratory of Clinical Biophysics, Faculty of Electrical Engineering, University of Ljubljana, Ljubljana, Slovenia | [4]Department of Otorhinolaryngology and Cervicofacial Surgery, University Medical Centre Ljubljana, Ljubljana, Slovenia | [5]Department of Chemical and Environmental Process Engineering, Budapest University of Technology and Economics, Budapest, Hungary | [6]Ambimass Kft., Budapest, Hungary | [7]Qamcom Central Europe, Budapest, Hungary | [8]Laboratory of Physics, Faculty of Electrical Engineering, University of Ljubljana, Ljubljana, Slovenia | [9]Department of Pharmaceutical Chemistry, Semmelweis University, Budapest, Hungary | [10]Center for Pharmacology and Drug Research & Development, Semmelweis University, Budapest, Hungary | [11]Waters Corporation, Cambridge, Massachusetts, USA | [12]Institute of Metals and Technology, Ljubljana, Slovenia | [13]Veterinary Faculty, University of Ljubljana, Ljubljana, Slovenia | [14]Faculty of Medicine, University of Ljubljana, Ljubljana, Slovenia

Correspondence: Gitta Schlosser (gitta.schlosser@ttk.elte.hu)

Received: 21 March 2026 | **Revised:** 10 June 2026 | **Accepted:** 15 June 2026

Keywords: ambient ionisation | extracellular vesicles | lipidomics | mass spectrometry | plasma characterisation

ABSTRACT

Remnants of erythrocyte removal from blood constitute therapeutic plasma—a water-based solution containing mainly platelets, extracellular vesicles (EVs), protein and lipid complexes and ions. Plasma-based therapies, including their use to accelerate wound healing in human and animal patients, are increasingly gaining prominence in regenerative medicine; however, methods for the optimal preparation of individual plasma are still under development. Rapid and accurate analysis of plasma composition is essential for the development of therapeutic applications and for ensuring the quality of plasma products before patient administration. This study of equine plasma presents a novel approach that utilises a newly developed automated well-plate sampling system using laser-assisted rapid evaporative ionisation mass spectrometry (LA-REIMS) for rapid plasma profiling under varying sample preparation conditions. This platform provided comprehensive lipidomic and metabolic analyses that gave insights into the molecular composition of plasma within seconds and without extensive sample preparation. The results indicated that specific phosphatidylcholines (PC(34:2), PC(36:2), PC(36:3)) and fatty acids were sensitive to centrifugation parameters, suggesting their potential as indicators of plasma stability and quality. The results were compared with the platelet and EV content of the plasma. The number density (n) of platelets and cellular fragments (P2 particles) was determined by flow cytometry (FCM), whereas EVs were characterised by interferometric light microscopy (ILM). The samples were imaged by scanning electron microscopy (SEM). A clear correlation was observed between n of P2 particles (but not of EVs) and lipid profiles, suggesting platelets' critical role in plasma composition. These findings emphasise the potential of the LA-REIMS platform for high-throughput, rapid plasma analysis, quality control and diagnostics. The system's ability to quickly assess plasma quality highlights its practical use in validating plasma prior to therapeutic applications.

This is an open access article under the terms of the Creative Commons Attribution-NonCommercial-NoDerivs License, which permits use and distribution in any medium, provided the original work is properly cited, the use is non-commercial and no modifications or adaptations are made.

© 2026 The Author(s). *Journal of Mass Spectrometry* published by John Wiley & Sons Ltd.

1 | Introduction

The application of blood-derived products, such as plasma, to damaged tissue areas has been found to be effective in accelerating wound healing and promoting the regeneration of injured ligaments and tendons [1–3]. The healing effect of plasma has primarily been attributed to platelets, which release various growth factors and inflammatory mediators into the extracellular environment that facilitate tissue repair [4]. However, recent findings have highlighted the potential significant role of extracellular vesicles (EVs) [5, 6]. EVs are cellular fragments that circulate freely in body fluids and serve as important mediators of cell-to-cell interactions [7, 8]. Since EVs are abundant in plasma [9, 10], they are thought to substantially contribute to tissue repair mechanisms. Therefore, a comprehensive understanding of plasma composition is essential for evaluating and monitoring therapeutic outcomes [11].

The comprehensive analysis of complex biological samples remains a significant challenge. Over the past few decades, mass spectrometry (MS) has become an indispensable tool in biological research and one of the leading methods for plasma analysis [12–15]. MS enables the identification and quantification of various plasma components such as phospholipids (e.g., phosphatidylcholines [PCs] and phosphatidylethanolamines [PEs]), fatty acids (FAs) and metabolites. Since even the smallest variations in plasma composition may indicate underlying physiological changes or reflect the effects of sample handling procedures, their monitoring is extremely important. Currently, MS coupled with chromatographic separation is the primary method for plasma analysis. However, the extensive and time-consuming sample preparation steps limit its suitability for rapid monitoring; therefore, alternative analytical approaches are needed.

Ambient ionisation MS techniques have gained prominence over the last two decades because they enable rapid molecular profiling with minimal sample preparation [16]. Methods such as desorption electrospray ionisation mass spectrometry (DESI-MS) have demonstrated the potential of ambient MS for the analysis of various biological samples such as plasma [17, 18]. More recently, laser-assisted rapid evaporative ionisation mass spectrometry (LA-REIMS) has emerged as another powerful ambient ionisation technique that overcomes the limitations of conventional MS methods [19, 20] and enables the direct analysis of complex biological samples [21]. The technique uses laser ablation for the evaporation of biological samples, which generates an aerosol composed of charged particles that is directly introduced into the atmospheric interface of the mass spectrometer for analysis (Figure 1). This method provides rich molecular profiles and facilitates the rapid detection of lipids and small metabolites [22]. Overall, LA-REIMS eliminates time-consuming sample preparation steps and thus provides a significant advantage in applications where rapid results are essential [23]. Furthermore, its compatibility with an automated well-plate sampling system makes it particularly suitable for high-throughput analyses. LA-REIMS has been widely applied in numerous fields [24], although clinical diagnostics remains its primary area of application. The technique has been extensively used for tissue analysis [22], successfully employed in the examination of cultured cell lines [21] and applied to the profiling of biological fluids [25]. Beyond clinical applications, the utility of LA-REIMS has been demonstrated in food analysis [26], microbial profiling [27] and the quality assessment of agricultural products [28].

In this study, we demonstrate that the newly developed automated high-throughput well plate sampling system using LA-REIMS [29] is highly effective for rapid plasma monitoring and provides valuable biological information about sample composition within seconds (Figure 1). To support the interpretation of the LA-REIMS data, complementary techniques were employed. Flow cytometry (FCM) was used to determine the number density (n) of platelets, interferometric light microscopy (ILM) was applied to measure the number density and hydrodynamic diameter (D_h) of EVs, and scanning electron microscopy (SEM) was used to visualise platelets and EVs. The results obtained by LA-REIMS were consistent with data generated by the complementary methods. Together, these findings highlight the platform's potential for high-throughput plasma monitoring and diagnostic applications.

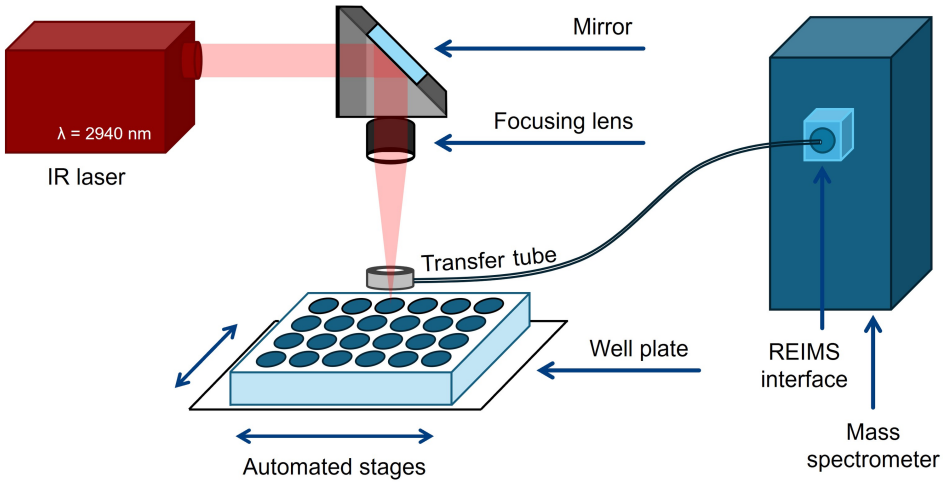


FIGURE 1 | Schematic representation of the automated high-throughput well-plate sampling system using LA-REIMS used for plasma analysis. The system integrates an infrared (IR) laser with a mirror and focusing lens for sample ablation from well plates positioned on motorised stages. The resulting aerosol is aspirated through a transfer tube and introduced into the mass spectrometer via a custom-built REMS interface.

10969888c, 2026, 8, Downloaded from https://analyticalsciencejournals.onlinelibrary.wiley.com/doi/10.1002/jms.70077 by Cochrane Slovenia, Wiley Online Library on [10/11/2026]. See the Terms and Conditions (https://onlinelibrary.wiley.com/terms-and-conditions) on Wiley Online Library for rules of use; OA articles are governed by the applicable Creative Commons License

2 | Materials and Methods

Blood was collected from an 18-year-old healthy mare (weighing approximately 500 kg) into a Compoflex 450 mL transfusion bag (Fresenius Kabi, Bad Homburg, Germany), which was prefilled with citrate phosphate dextrose adenine (CPDA) solution as an anticoagulant. The collection was performed by puncture of the jugular vein using a 15-gauge (1.8 × 38 mm) needle connected directly to the transfusion bag. Upon connection, blood began to flow steadily into the bag. Following collection, the blood was gently homogenised by carefully squeezing the bag to ensure even distribution of its components. The collected blood was then aliquoted into 3 mL tubes by gently pushing it through the connected plastic tubing.

Blood samples were centrifuged at 18°C under various centrifugal forces and durations to separate plasma and evaluate the effects of centripetal acceleration and centrifugation time on plasma yield and quantity. First, blood samples were centrifuged at 41 × *g* (the lowest possible centrifugal force) for 2, 2.5, 3, 3.5, 4, 4.5, 5, 6, 8 and 10 min to assess the sedimentation speed of equine plasma. Second, blood samples were centrifuged at 50, 60, 70, 80, 90, 100, 110, 120, 130, 140 and 150 × *g* for 5 min to examine the role of centripetal acceleration in sedimentation. After each centrifugation, plasma was removed approximately 3 mm above the visible erythrocyte boundary using a pipette and transferred into 1.5 mL Eppendorf tubes.

Plasma samples were stored at three different temperatures: in the fridge (at 4°C), at −20°C and −80°C for 295 days prior to analysis. The samples were then thawed and analysed without any further sample preparation using ambient ionisation MS.

Samples were analysed using an automated well-plate sampling system using LA-REIMS coupled to a Xevo G2-XS Q-TOF (quadrupole time-of-flight) mass spectrometer (Waters Corporation, Milford, MA, USA). A 96-well V-bottom microplate (Greiner Bio-One, Kremsmünster, Austria), with each well containing 100 μL of plasma, was positioned in a holder socket, and motorised X-Y-Z stages were used for precise alignment during the measurement process. Sample ablation was performed using a commercially available Opolette HE 2940 Optical Parametric Oscillator (Opotek LLC, Carlsbad, CA, USA) laser, operating at a wavelength of 2940 nm, and pulse peak energy of 6 mJ at a frequency of 20 Hz. The optical path consisted of a mirror (PFE-P01) and a plano-convex CaF_2 focusing lens with 50 mm focal length (LA5763) (Thorlabs Inc., Newton, NJ, USA). The aerosol generated above the sample was aspirated using a custom-built Direct REIMS interface (Waters Research Center, Budapest, Hungary) [19], with a 2 m surgical Tygon tube with an outer diameter of 2.2 mm serving as the aspiration conduit. The aspirated aerosol was subsequently mixed with a continuous flow of propan-2-ol (Merck, Darmstadt, Germany) containing 0.1 ng/μL leucine enkephalin (Thermo Fisher Scientific, Waltham, MA, USA), which was introduced directly in front of the mass spectrometer's inlet capillary at a flow rate of 150 μL/min [30].

Data acquisition was conducted in negative ion mode with a scan time of 0.5 s and a mass-to-charge (*m*/*z*) range of 50–1200. Three parallel measurements were performed for each sample, with eight scans acquired per measurement, which resulted in 24 scans in total. The acquired scans were evaluated based on the signal profile. Scans corresponding to the initial signal rise and final signal decay phases were excluded, and only scans from the stable signal plateau exhibiting similar signal intensities were retained. After this quality assessment, 18 scans were selected and averaged to analyse lipid relative intensities. The acquired data were processed using our in-house developed software, Abstract Model Builder (AMX, [Beta] version 1.0.58.0, Waters Research Center, Budapest, Hungary), employing multivariate statistical analyses, including principal component analysis (PCA) followed by linear discriminant analysis (LDA). Data visualisation was performed using MassLynx V4.2 (Waters Corporation, Wilmslow, United Kingdom), and manual evaluation was carried out using the top 50 most abundant peaks. Molecular identification was achieved through exact mass measurements, tandem mass spectrometry (MS/MS) (Figures S1–S5) and lipidmaps.org database [31].

To assess the similarity between different centrifugation conditions within the PCA/LDA space, Euclidean distances were calculated in the PCA space. Key peaks contributing to the most significant differences were identified using a supervised classification method, linear support vector classification (LSVC). An *F*-test was applied with a significance of 0.05 to determine whether the variances between the two samples were equal. If variances were unequal, a Welch test was performed to determine the significance of the means differing (*p*-value); if variances were equal, a *t*-test was used instead. Fold change values were calculated by dividing the average intensity of a specific spectral bin in Class A by the corresponding bin in Class B, and the result was rounded to two decimal places. This means that a fold change value is greater than one if the average intensity in Class B was lower than in Class A, whereas a value less than one suggests the opposite.

For FCM, plasma was diluted twentyfold in phosphate-buffered (physiological) saline. P2 particles are defined by gating within the FCM forward/side scattering diagram below the region of erythrocytes [32]. They contain mostly platelets but also larger cellular fragments deriving from blood cells. *n* of P2 particles in the plasma samples was determined using a MACSQuant Analyzer flow cytometer (Miltenyi Biotec, Bergisch Gladbach, Germany). The following instrument settings were used: forward scatter (FSC) at 458 V, side scatter (SSC) at 467 V with a trigger set to 1.48, B3 at 300 V and R1 at 360 V. Particles were detected based on the FSC and SSC parameters. Before the measurements, samples were gently mixed by pipetting to ensure homogeneity, and a total of 20 000 events per well were recorded. Data analysis was performed using MACSQuantify software, version 2.5 (Miltenyi Biotec, Bergisch Gladbach, Germany).

For imaging by SEM, EVs were isolated from plasma by centrifugation. A total of 250 μL of plasma aliquots were transferred to Eppendorf tubes and centrifuged at 17 570 × g for 10 min at room temperature using a Centric 200R centrifuge equipped with a Lilliput rotor (Domel, Železniki, Slovenia). After centrifugation, 200 μL of the supernatant was carefully removed and replaced with phosphate-buffered saline (PBS). The samples were resuspended and centrifuged again under the same conditions. Following this second centrifugation, 200 μL of the

10969888c, 2026, 8, Downloaded from https://analyticalsciencejournals.onlinelibrary.wiley.com/doi/10.1002/jms.70077 by Cochrane Slovenia, Wiley Online Library on [10/11/2026]. See the Terms and Conditions (https://onlinelibrary.wiley.com/terms-and-conditions) on Wiley Online Library for rules of use; OA articles are governed by the applicable Creative Commons License

supernatant was discarded. The samples shown in Figure 4A,B were loaded onto 0.05 μm mixed cellulose esters (MCE) filters (MF-Millipore, ref. VMWP01300) (Merck, Darmstadt, Germany) and incubated in 1% OsO_4 for 1 h. After the removal of osmium, the filter was taken out of the holder and further treated in a 24-well plate with sequential bath solution changes. The samples were washed three times with distilled water, dehydrated through an ethanol series (30%, 50%, 70%, 80%, 90% and absolute ethanol), treated with hexamethyldisilazane (HMDS) in incremental concentrations (30%, 50% mixtures with absolute ethanol, followed by pure HMDS) and air-dried. Samples were then sputtered with Au/Pd using a PECS Gatan 682 sputter coater and examined with a JSM-6500F Field Emission Scanning Electron Microscope (JEOL Ltd., Tokyo, Japan). Samples presented in Figure 4C,D were suspension-fixed in 1% glutaraldehyde dissolved in PBS/citrate buffer for 60 min at 22°C prior to OsO_4 treatment. These were sputtered with Au and analysed using a LEO Gemini 1530 scanning electron microscope (LEO, Oberkochen, Germany).

The average n and D_h of EVs were measured by ILM using the Videodrop system (Myriade, Paris, France) [9]. The signal from the media (saline) was below the detection limit, and a threshold value of 4.2 was applied for analysis. Seven microlitres of the samples was placed between cover glasses and illuminated by 2 W of blue LED light. Scattered light from individual particles interfered with the incoming light, and the resulting interference patterns were captured using a high-resolution, high-speed complementary metal-oxide-semiconductor camera through a bright-field microscope objective. The hydrodynamic parameter of each particle was estimated by tracking its position over time within the recorded video. Particle motion was assumed to follow Brownian motion, driven by collisions with surrounding particles. The diffusion coefficient (D) of the motion was estimated based on the mean square displacement of the particle between consecutive frames recorded at time intervals. D_h was then calculated assuming spherical particles, using the Stokes–Einstein equation. Each particle included in the analysis was individually tracked and processed, with background light signals subtracted from each image. All image and video data processing was performed using the QVIR 2.6.0 software (Myriade, Paris, France).

3 | Results

Blood samples were subjected to various centripetal accelerations and durations to optimise plasma isolation and evaluate the effects of centrifugation parameters on the lipidomic and metabolic profile of the plasma. Because of a relatively fast sedimentation of erythrocytes in equine blood, the centripetal acceleration of the centrifuge rotor was set to its minimum (41 × g, where g is the acceleration of the Earth's gravity) for different time intervals. Subsequently, the effects of increasing centrifugal forces (50–150 × g) were assessed. Plasma aliquots were stored at three different temperatures (4°C, −20°C, −80°C) and analysed using the newly developed automated sampling system using LA-REIMS.

After storing plasma aliquots at different temperatures, an initial assessment was performed to evaluate the impact of storage conditions on plasma integrity and suitability for further analysis. Visual inspection revealed no signs of degradation in any of the samples. However, mass spectrometric analysis showed that plasma stored at 4°C exhibited markedly different metabolic and lipidomic fingerprints compared with samples stored at −20°C and −80°C (Figure S6). Samples stored at 4°C showed significantly elevated signal intensities in the lower m/z region, which is primarily associated with small metabolites such as sugars and FAs. In some cases, the intensity of the metabolic signal even exceeded that of the lipidomic region. This divergence is likely due to incomplete metabolic arrest at 4°C, which allows continued enzymatic activity and oxidative degradation. As a result, metabolite levels may be altered, and degradation products may be formed. These findings suggest that 4°C is not suitable for the prolonged storage of plasma, as it causes significant changes in the lipidomic profile. Based on these observations, only samples stored at −20°C and −80°C were examined for further lipidomic analysis.

To evaluate similarities and differences between samples, PCA/LDA analyses were used to assess clustering and separation in multivariate space. Then, all sample classes were compared to identify major lipidomic differences, and the relative intensities of distinguishing lipids were determined for each condition.

To assess the effect of centrifugation time on plasma composition, samples were centrifuged at 41 × g for varying durations. PCA/LDA analysis showed that samples centrifuged for 2 and 2.5 min were more similar to each other (PCA space distance of 0.636 [−20°C] and 0.282 [−80°C]) and different (PCA space distance of 1.011–1.797 [−20°C] and 0.306–1.072 [−80°C]) compared with those centrifuged for longer periods (3–10 min). Relative lipid intensities were initially lower in samples centrifuged for 3–4 min, which was followed by a notable increase between 5 and 6 min. This suggests that lipids contributing to the major differences were more abundant in samples centrifuged for slightly over 5 min than in those centrifuged for shorter durations.

Based on these findings, samples were subjected to different g-centripetal accelerations of the centrifuge rotor for a constant duration of 5 min to examine the effect of centrifugal force on lipidomic profiles. PCA/LDA analysis revealed continuous changes up to 90 × g, above which samples centrifuged at 100–150 × g displayed a higher degree of similarity. The relative intensities of the lipids responsible for these changes increased gradually up to 80 × g and then started decreasing at 90 × g, which continued until 150 × g. The results are demonstrated by the m/z 820.563 peak corresponding to the PC(36:2) lipid responsible for the major differences (Figure 2). The reproducibility of these lipid relative intensity values is further supported by relative standard deviation (RSD %) and standard error values, which are presented in the Table S1.

Building on these findings, to further explore the impact of optimised centrifugation conditions (5 min at 80 × g), we proceeded to the detailed molecular analysis of the samples. The resulting mass spectra displayed a distinct lipid pattern characteristic of horse plasma, predominantly featuring PCs as the main membrane lipids (Figure 3). Additionally, sphingomyelins (SM) and PEs were also identified. These lipids were the

10969888c, 2026, 8, Downloaded from https://analyticalsciencejournals.onlinelibrary.wiley.com/doi/10.1002/jms.70077 by Cochrane Slovenia, Wiley Online Library on [10/11/2026]. See the Terms and Conditions (https://onlinelibrary.wiley.com/terms-and-conditions) on Wiley Online Library for rules of use; OA articles are governed by the applicable Creative Commons License

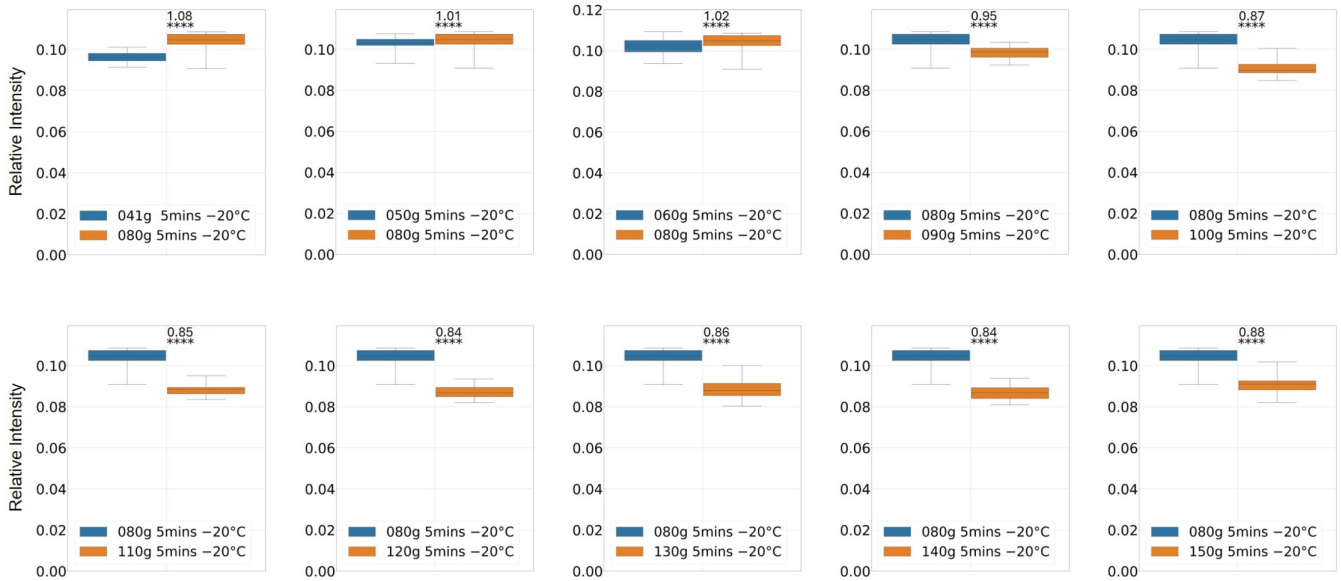


FIGURE 2 | The relative intensities of m/z 820.563 peak corresponding to PC(36:2), which is responsible for the main differences observed across different centripetal accelerations (samples stored at −20°C), with a significance level **** indicating $p < 0.0001$, and fold change values (with > 1 indicating greater intensity average of the higher centrifugation force class and < 1 indicating greater intensity average of the lower centrifugation force class).

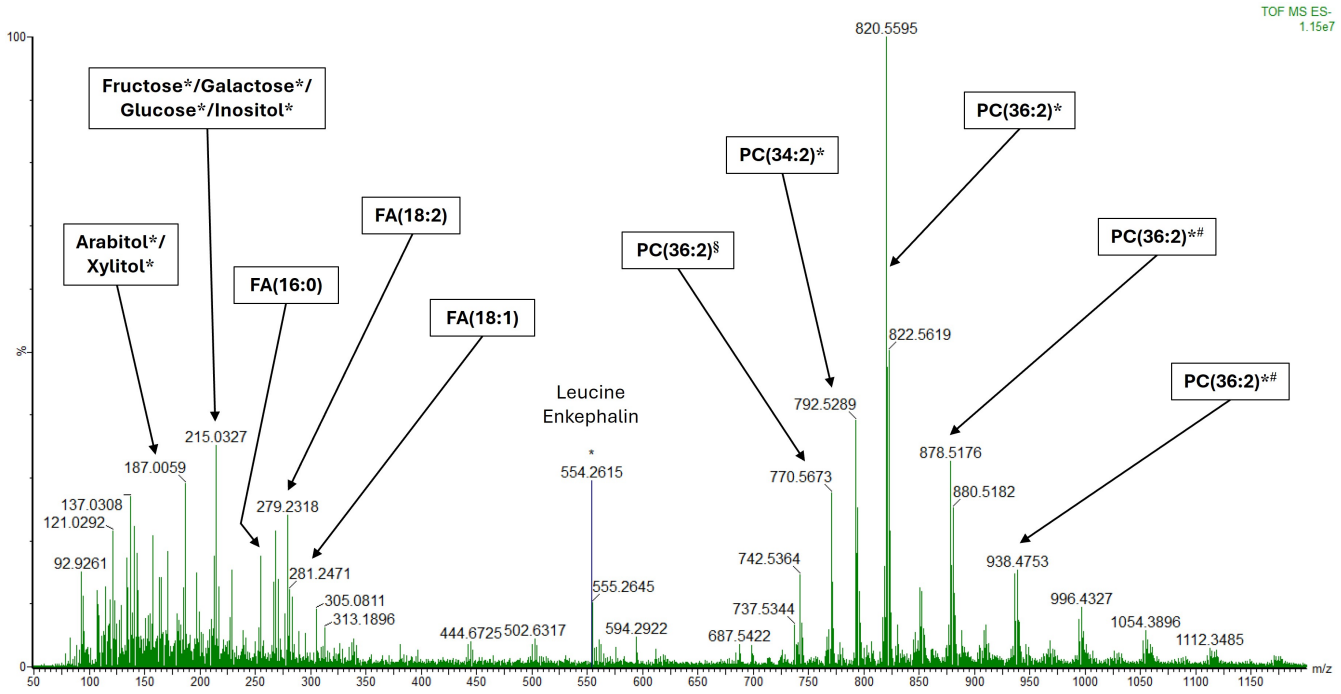


FIGURE 3 | Mass spectrum of equine plasma under optimal conditions (5 min at 80 × *g*, average of five scans) measured by LA-REIMS. There is a distinct lipidomic profile in the 600–900 m/z region, characterised by various lipids detected in different adduct forms. The lower m/z region is abundant in metabolites, mainly sugars and fatty acids. Symbols refer to adduct types: * denotes $[M+Cl]^-$, § represents $[M - CH_3]^-$, # indicates a NaCl adduct.

primary contributors to the observed differences across varying centrifugation times and forces. These findings indicate the central role of these lipids in plasma lipidomic variation.

The detailed analysis of the lipidomic profiles revealed several lipids in various adduct forms in the samples (Table 1). SM(34:1;O2), PC(34:2) and PC(36:2) were present in both $[M - CH_3]^-$ and $[M+Cl]^-$ forms, whereas CerPE(36:1;O2), PE(36:2) and PE(38:2) appeared in the form of $[M-H]^-$. For both PCs, but particularly for PC(36:2), a series of NaCl adducts was observed in the higher m/z regions. Additionally, a peak at m/z 818.541, identified as PC(36:3), was noted as a significant contributor to the observed lipidomic variability. Taken together, these lipids were identified as key contributors to the observed lipidomic

10969888c, 2026, 8, Downloaded from https://analyticalsciencejournals.onlinelibrary.wiley.com/doi/10.1002/jms.70077 by Cochrane Slovenia, Wiley Online Library on [10/11/2026]. See the Terms and Conditions (https://onlinelibrary.wiley.com/terms-and-conditions) on Wiley Online Library for rules of use; OA articles are governed by the applicable Creative Commons License

TABLE 1 | The major peaks identified in the lipidomic region (600–900 *m*/*z*) of equine plasma, their measured and accurate *m*/*z* values, mass errors, the corresponding identified lipids and their respective adduct forms.

m/*z* (measured)	*m*/*z* (accurate)	Mass error/ppm	Lipids	Adduct
687.542	687.544	−2.91	CerPE(36:1;O2)	$[M-H]^-$
			SM(34:1;O2)	$[M-CH_3]^-$
737.535	737.537	−2.71	SM(34:1;O2)	$[M+Cl]^-$
742.537	742.539	−2.69	PE(36:2)	$[M-H]^-$
			PC(34:2)	$[M-CH_3]^-$
770.567	770.571	−5.19	PE(38:2)	$[M-H]^-$
			PC(36:2)	$[M-CH_3]^-$
792.529	792.532	−3.79	PC(34:2)	$[M+Cl]^-$
818.541	818.547	−7.33	PC(36:3)	$[M+Cl]^-$
820.559	820.563	−4.87	PC(36:2)	$[M+Cl]^-$
878.518	878.522	−4.55	PC(36:2)	$[M+Cl+NaCl]^-$

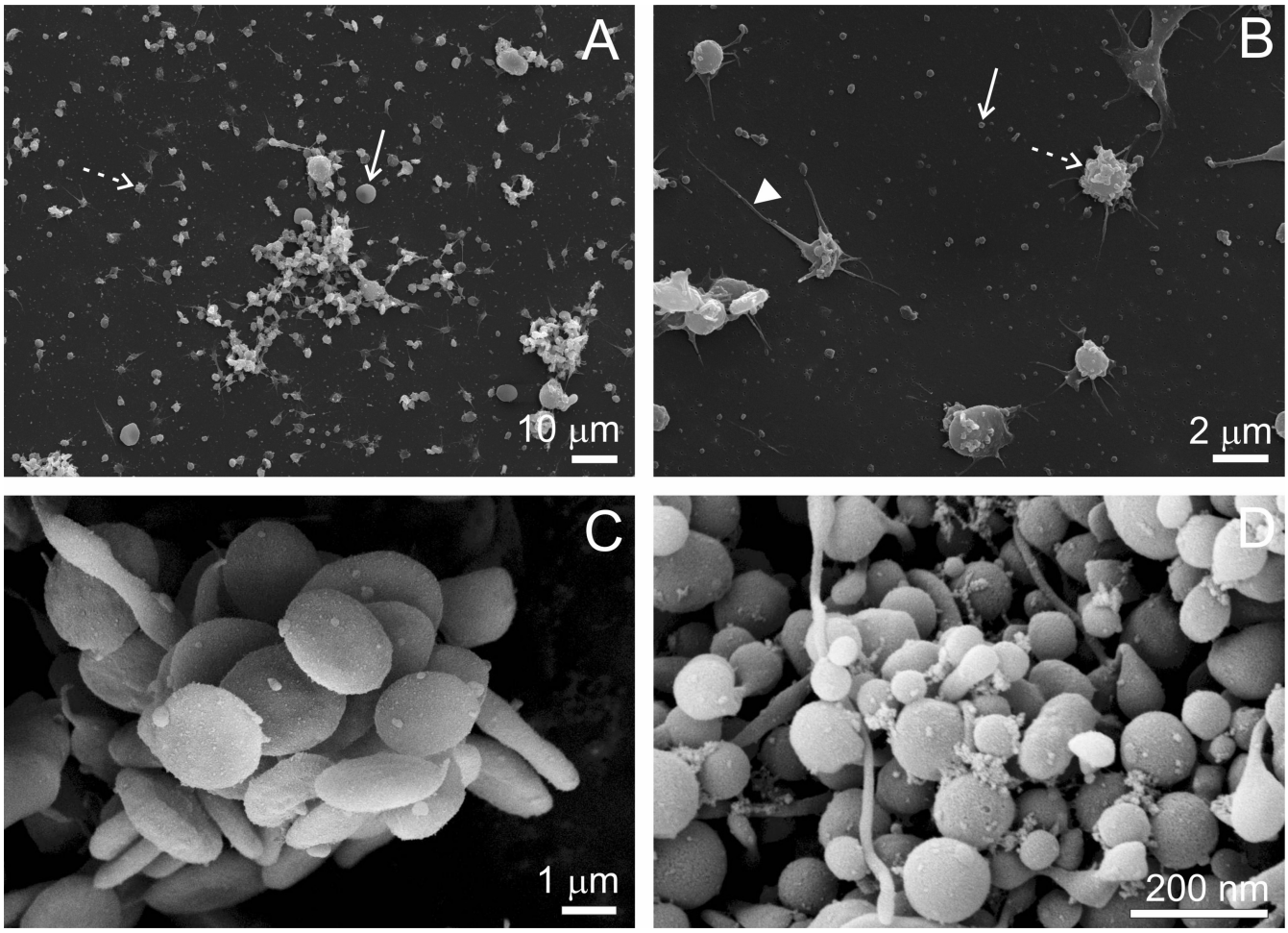


FIGURE 4 | (A) Isolate of extracellular vesicles from equine plasma. The arrow points to an erythrocyte. (B) A close-up of EVs isolated from plasma showing activated platelets (dashed white arrow) and numerous EVs (white arrow). The white triangle points to a tubular protrusion of the platelet membrane. (C) Resting platelets from plasma. (D) EVs isolated from plasma.

10969888c, 2026, 8, Downloaded from https://analyticalsciencejournals.onlinelibrary.wiley.com/doi/10.1002/jms.70077 by Cochrane Slovenia, Wiley Online Library on [10/11/2026]. See the Terms and Conditions (https://onlinelibrary.wiley.com/terms-and-conditions) on Wiley Online Library for rules of use; OA articles are governed by the applicable Creative Commons License

changes across different centrifugation times and centrifugal forces.

In the lower mass range, multiple metabolites were identified, primarily sugars and FAs, which contributed significantly to the changes observed under different centrifugation conditions. Sugars such as arabytol/xylitol were detected in the form of a chloride adduct as $[C_5H_{12}O_5+Cl]^-$, whereas hexoses such as fructose/galactose/glucose/inositol were identified as $[C_6H_{12}O_6+Cl]^-$. Among the FAs, FA(16:0), FA(18:1) and FA(18:0) represented the most abundant compounds, along with the less abundant FA(16:1) and FA(18:0), together reflecting varying chain lengths and degrees of saturation.

Overall, these results demonstrate the effectiveness of the newly developed automated system using LA-REIMS for rapid and detailed plasma monitoring. The platform provided information about each sample in 3 s, and the identified metabolic and lipidomic changes highlighted the system's capability to detect subtle variations under different preparation conditions. The results confirmed 5 min at $80\times g$ as optimal for equine plasma preparation.

To further explore plasma composition, plasma components such as platelets and EVs were examined with complementary methods. Because of their small size and fragility, combined with the physical properties of the plasma matrix, EVs are difficult to visualise directly. Therefore, EV isolates were prepared by further centrifugation at higher centripetal acceleration and washing of the samples. SEM imaging of the isolates revealed distinct plasma components; EVs were visualised (Figure 4A, dashed white arrow, and B, white arrow) along with activated platelets. Numerous sub-micron-sized globular EVs were observed (Figure 4B, white arrow, and Figure 4D), along with thin tubular protrusions (Figure 4B, white triangle) from activated platelets (Figure 4B, dashed white arrow). Resting platelets displayed their characteristic disc-like morphology (Figure 4C) in comparison with the activated forms in the isolates.

SEM images so far provide the best information on the three-dimensional structure of plasma constituents. Figure 4A shows residual cells (singular erythrocytes and numerous platelets), whereas Figure 4B reveals the presence of even smaller particles—EVs. Also, Figure 4C shows that the platelets in the sample were activated by exhibiting thin protrusions that may pinch off and decay into globular vesicles. Figure 4D shows that EVs in the isolates are heterogeneous in size and shape. As the preparation of samples for SEM is challenging and time-consuming, this technique is rarely used in identifying the particles in the samples. Furthermore, the procedure (described in detail in Section 2) affects the samples; the concern is mostly for losing particles in rinsing and pipetting. Nevertheless, the observations (Figure 4) give insight into processes leading to the fragmentation of cells in the samples.

Platelet number density (n) in dependence on the centripetal acceleration of the centrifuge rotor showed a peak at $80\times g$ (Table 2). Platelet n gradually increased up to this condition, followed by a steady decline with further increases in centripetal acceleration. As both the lipidomic signal and platelet n exhibited a non-monotonic dependence on centripetal acceleration, this relationship cannot be described by either Pearson or Spearman correlation analysis, which assume linear and monotonic dependence, respectively. We performed a more detailed analysis by correlating the normalised lipid signal with the normalised platelet number density. Second-order polynomials were fitted as $y_i=a_i\,(g-g_{0i})^2+d_i$ with respective parameters a_i, g_{0i} and d_i, where i stands for the lipid signal (l) and platelet number density (n) ($a_l=a_n=-0.0013$, $g_{0,l}=65.3$, $g_{0i}=86.5$, $d_{i,l}=9.93$, $d_{i,n}=11.5$). Dependency of normalised lipid signal/platelet number density on $(g-g_{0i})^2$ showed statistically significant correlation (Pearson $r=-0.97$, $p<10^{-6}$, Spearman $\rho=-0.83$,

TABLE 2 | Centrifugation parameters and their effects on lipid relative intensities, platelet number density (n), extracellular vesicles (EVs) number density (n) and hydrodynamic diameter (D_h).

Centrifugation force/g	Time/min	Lipid relative intensities	n (platelets) $\times 10^9$/mL	n (EVs) $\times 10^9$/mL	D_h (EVs) /nm
41	5	0.92	0.892	9.19	155
50	5	0.99	0.961	9.96	145
60	5	0.98	1.043	11.72	156
70	5	—	1.120	11.47	159
80	5	1	1.148	10.31	157
90	5	0.95	1.130	12.72	156
100	5	0.87	1.097	13.59	188
110	5	0.85	—	17.80	176
120	5	0.84	—	17.21	178
130	5	0.86	—	24.00	172
140	5	0.84	—	14.65	176
150	5	0.88	—	20.55	181

10969888c, 2026, 8, Downloaded from https://analyticalsciencejournals.onlinelibrary.wiley.com/doi/10.1002/jms.70077 by Cochrane Slovenia, Wiley Online Library on [10/11/2026]. See the Terms and Conditions (https://onlinelibrary.wiley.com/terms-and-conditions) on Wiley Online Library for rules of use; OA articles are governed by the applicable Creative Commons License

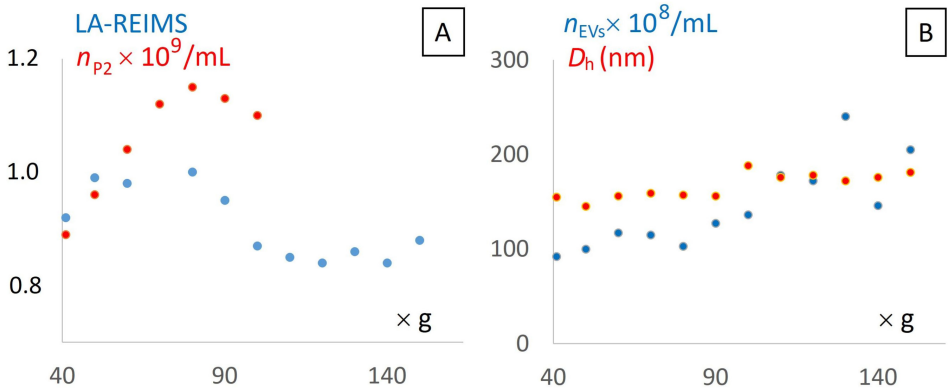


FIGURE 5 | (A) Relationship between LA-REIMS relative lipid intensities (blue) and platelet number density (n_{P2}, red) under varying centripetal accelerations (×g). Both parameters exhibited similar responses to centrifugation conditions, reaching a maximum at 80×g before declining. However, n was unavailable for higher centripetal accelerations due to measurement limitations. (B) Extracellular vesicle number density (n_{EVs}, blue) and D_h (red) as functions of varying centripetal accelerations (×g). The associations between n_{EVs} and centripetal acceleration, as well as between D_h and centripetal acceleration, were statistically significant according to both Pearson and Spearman correlation analyses (Pearson r=0.83 and 0.80, respectively, with p=0.002 and 0.003; Spearman ρ=0.91 and 0.78, respectively, with p=0.0001 and 0.0046). Furthermore, a significant association was observed between n_{EVs} and D_h (Pearson r=0.66, p=0.027; Spearman ρ=0.72, p=0.012).

p=0.0008). These results further support the interpretation that both parameters respond similarly to centrifugation conditions (Figure 5A). SEM imaging confirmed the presence of EVs in the plasma, and ILM revealed vesicles with diameters ranging from 140 to 190 nm. Although EVs' n and hydrodynamic diameter (D_h) varied, no direct correlations of these parameters with each other (Figure 5B) or with the lipidomic profiles obtained by LA-REIMS were found.

The combined analysis of platelets, EVs and lipid profiles revealed that centrifugation at 80×g for 5 min preserved lipid stability and minimised mechanical stress on plasma components. Prolonged centrifugation resulted in reduced platelet number density and lipid content. These findings highlight the importance of optimised preparation protocols to maintain plasma integrity and ensure reproducibility in both therapeutic and diagnostic applications.

4 | Discussion

Lipids play diverse and critical roles in the body: They contribute to the maintenance of cellular structure, the regulation of signalling pathways and overall metabolic balance. Among lipid species, PCs are the major constituents of biological membranes, where they play key roles in maintaining membrane stability and protecting cells from oxidative stress [33]. Alterations in PC metabolism have been associated with various diseases, such as cardiovascular diseases [34, 35], neurodegenerative disorders [36, 37] and cancers [38]. Therefore, these molecules may serve as potential biomarkers for disease detection and progression monitoring. Although plasma itself does not contain cell membranes, it carries numerous lipid molecules that reflect the metabolic state of the cells from which they originate. Thus, the lipid composition of plasma is a sensitive indicator of both cell-derived changes and the effects of sample handling.

This study demonstrates the potential of the automated well-plate sampling system using LA-REIMS as an efficient and reliable tool for plasma analysis. LA-REIMS measurements were complemented by FCM, ILM and SEM, which enabled comprehensive characterisation of plasma components and validated the robustness of the LA-REIMS results.

Our findings highlight that centrifugation parameters—such as centripetal acceleration and duration—play a significant role in maintaining plasma integrity. Optimal results were obtained at 80×g for 5 min for equine plasma, where lipid stability was maintained, and the degradation of residual cellular components remained minimal. Moreover, lipids with the highest relative intensities, such as PC(34:2), PC(36:3) and PC(36:2), contributed significantly to the observed lipidomic variability. Although their precise physiological functions in equine plasma have not yet been elucidated, these lipids are well documented in mammalian systems [39]. Alterations in their abundance have been linked to numerous pathological conditions, including cancer [40, 41], atherosclerosis [42] and neurodegenerative diseases [43, 44]. These lipids were highly sensitive to sample processing conditions and reflected changes in plasma composition and integrity within the investigated sample set. Although their specific roles in equine biology remain to be clarified, their consistent detection and observed sensitivity to centrifugation conditions suggest that they may have potential as indicators of plasma quality in veterinary applications. However, further studies involving larger numbers of animals are required to evaluate their biological significance and broader applicability.

In addition, distinct signals from sugars and FAs indicate that the metabolic region reflects plasma integrity and is strongly influenced by centrifugation and storage conditions. Therefore, variations in FA profiles may serve as indicators for optimising plasma sample processing.

Moreover, the investigation of lipidomic and metabolic changes is crucial for understanding lipid metabolism in health and disease. PCs play a central role in metabolic pathways, and fluctuations in their levels or composition may indicate underlying disease-related biochemical changes [45]. Correlating lipidomic

10969888c, 2026, 8, Downloaded from https://analyticalsciencejournals.onlinelibrary.wiley.com/doi/10.1002/jms.70077 by Cochrane Slovenia, Wiley Online Library on [10/11/2026]. See the Terms and Conditions (https://onlinelibrary.wiley.com/terms-and-conditions) on Wiley Online Library for rules of use; OA articles are governed by the applicable Creative Commons License

profiles with clinical outcomes may therefore contribute to the development of comprehensive diagnostic and monitoring tools.

Our observations revealed a clear correlation between lipid intensity and platelet n, which highlights the importance of platelets in contributing to the lipidomic profile of plasma. This correlation suggests that platelets, as cellular reservoirs of lipids, significantly influence plasma composition, and their stability under optimised centrifugation conditions ensures accurate lipid analysis. LA-REIMS enabled the rapid detection of these relationships and provided molecular information consistent with the complementary methods in a markedly shorter time.

Although EVs were successfully isolated and visualised using SEM, confirming their presence in the plasma, their lipid contribution to the overall plasma composition appeared to be less significant compared with that of the platelets. Despite the variability observed in EV n and D_h under different centrifugation conditions, no direct correlation between these parameters and the lipidomic profiles was found. However, Figure 5B shows that both n and D_h of EVs increased with higher centripetal acceleration. It is likely that the fragmentation of platelets in shear stress imposed at the walls of the tube is the source of the pool of EVs [46, 47]. Notably, the fragments are, on average, larger at higher centripetal accelerations, which strongly supports this hypothesis.

Besides platelets and EVs, lipoproteins are another major source of lipids in plasma, as they are the main lipid particles in blood-derived samples [48–51]. The size of lipoproteins, assessed by nuclear magnetic resonance (21 nm for low-density lipoproteins, 9 nm for high-density lipoproteins and 47–49 nm for very-low-density lipoproteins) [52], is under the detection limit of ILM (about 80–500 nm). However, lipoproteins may interact with EVs [49, 50, 53], and the proportion of lipoproteins in plasma may depend on sample processing [54, 55]. These findings highlight the need for further methodological advancements to avoid fluctuations in EV n and D_h, and this way better capture the lipidomic contributions of EVs.

The motion of cells during centrifugation of blood is rather complex. Initially, particles are distributed homogeneously throughout the blood in the tube. Erythrocytes, due to their size, move the fastest towards the bottom of the tube. As they concentrate, they push plasma, which carries smaller particles (such as platelets and fragments), in the opposite direction [32]. This process is further enhanced by the formation of erythrocyte rouleaux that form channels in which plasma moves upwards. This process ceases when erythrocytes are closely packed to present a pellet, and plasma rich in smaller particles is formed above the boundary of erythrocytes. Although the platelets are no longer pushed upwards, the centrifugal force pulls them towards the erythrocyte boundary, diminishing their number density in the upper part of the tube. When plasma is collected, the part above the erythrocyte boundary (about 3–5 mm) remains in the tube. Thus, the plasma that is used for therapeutic means may become poor in platelets if the centrifugation is either too long or too strong. Our results indicate that the lipid content follows that of the platelets, but further research is needed to better understand interactions between particles during blood and plasma centrifugation.

The study also emphasises the importance of standard protocols for sample preparation, storage and reproducibility. Our findings indicated that plasma stored at −20°C or −80°C maintained lipid stability, whereas storage at 4°C resulted in significant lipidomic alterations and is therefore not suitable for prolonged storage.

Overall, the integration of the automated well-plate sampling system using LA-REIMS into plasma analysis is a novel approach that provides detailed molecular information about the samples within seconds. The method significantly reduces analysis time compared with conventional procedures, which makes it well-suited for high-throughput applications. The results were validated through complementary methods, which confirmed the system's accuracy and reliability, and highlighted its suitability for optimising sample handling processes. Further studies involving larger sample cohorts will be necessary to evaluate its broader applicability in veterinary and clinical diagnostic settings.

Our findings demonstrate the potential of LA-REIMS as a rapid and reliable platform for plasma lipidomic analysis. Its streamlined workflow and capacity for high-throughput molecular profiling make it a promising tool for both research and future diagnostic applications.

Funding

Prepared with the professional support of the Doctoral Student Scholarship Program of the Co-operative Doctoral Program of the Ministry of Innovation and Technology, financed from the National Research, Development and Innovation Fund. This project was supported by the Lendület (Momentum) Program of the Hungarian Academy of Sciences (HAS, MTA). Project no. SNN 148580 has been implemented with the support provided by the Ministry of Innovation and Technology of Hungary from the National Research, Development and Innovation Fund, financed under the SNN_24 funding scheme, and by the Slovenian Research and Innovation Agency (ARIS) (grant numbers P2-0132, P2-0232, P3-0388, P4-0053 and J3-60063).

Ethics Statement

The study was approved by the Animals in Experiments Welfare Commission of the Veterinary Faculty, University of Ljubljana, approval number 18-3/2022-1.

Data Availability Statement

The authors have nothing to report.

References

1. E. T. Daif, "Effect of Autologous Platelet-Rich Plasma on Bone Regeneration in Mandibular Fractures," *Dental Traumatology* 29, no. 5 (2012): 399–403, https://doi.org/10.1111/edt.12021.

2. B. K. Manne, F. Denorme, E. A. Middleton, et al., "Platelet Gene Expression and Function in Patients With COVID-19," *Blood* 136, no. 11 (2020): 1317–1329, https://doi.org/10.1182/blood.2020007214.

3. K. Troha, D. Vozel, M. Arko, et al., "Autologous Platelet and Extracellular Vesicle-Rich Plasma as Therapeutic Fluid: A Review," *International Journal of Molecular Sciences* 24, no. 4 (2023): 3420, https://doi.org/10.3390/ijms24043420.

10969888c, 2026, 8, Downloaded from https://analyticalsciencejournals.onlinelibrary.wiley.com/doi/10.1002/jms.70077 by Cochrane Slovenia, Wiley Online Library on [10/11/2026]. See the Terms and Conditions (https://onlinelibrary.wiley.com/terms-and-conditions) on Wiley Online Library for rules of use; OA articles are governed by the applicable Creative Commons License

4. J. Etulain, "Platelets in Wound Healing and Regenerative Medicine," *Platelets* 29, no. 6 (2018): 556–568, https://doi.org/10.1080/09537104.2018.1430357.

5. D. Vozel, D. Božič, M. Jeran, et al., "Treatment With Platelet- and Extracellular Vesicle-Rich Plasma in Otorhinolaryngology—A Review and Future Perspectives," in *Advances in Biomembranes and Lipid Self-Assembly* (Academic Press, 2020), 119–153, https://doi.org/10.1016/bs.abl.2020.05.003.

6. D. Vozel, D. Božič, M. Jeran, et al., "Autologous Platelet- and Extracellular Vesicle-Rich Plasma Is an Effective Treatment Modality for Chronic Postoperative Temporal Bone Cavity Inflammation: Randomized Controlled Clinical Trial," *Frontiers in Bioengineering and Biotechnology* 9 (2021): 9, https://doi.org/10.3389/fbioe.2021.677541.

7. M. Yáñez-Mó, P. R. M. Siljander, Z. Andreu, et al., "Biological Properties of Extracellular Vesicles and Their Physiological Functions," *Journal of Extracellular Vesicles* 4, no. 1 (2015): 27066, https://doi.org/10.3402/jev.v4.27066.

8. J. A. Welsh, D. C. Goberdhan, L. O'Driscoll, et al., "Minimal Information for Studies of Extracellular Vesicles (MISEV2023): From Basic to Advanced Approaches," *Journal of Extracellular Vesicles* 13, no. 5 (2024): e12451, https://doi.org/10.1002/jev2.12404.

9. A. Romolo, Z. Jan, A. B. Zavec, et al., "Assessment of Small Cellular Particles From Four Different Natural Sources and Liposomes by Interferometric Light Microscopy," *International Journal of Molecular Sciences* 23, no. 24 (2022): 15801, https://doi.org/10.3390/ijms232415801.

10. B. Korenjak, A. Tratenšek, M. Arko, et al., "Assessment of Extracellular Particles Directly in 613 Human and 163 Canine Diluted Plasma and Blood Samples by Interferometric Light Microscopy," *Cells* 13, no. 24 (2024): 2054.

11. G. Schlosser, A. Molnár, D. Papp, et al., "Omics Mass Spectrometry Analysis of Canine Plasma," in *Proceedings of 10th Socratic Lectures* (Proc Socratic Lect, 2024), https://doi.org/10.55295/psl.2024.i11.

12. R. Aebersold and M. Mann, "Mass Spectrometry-Based Proteomics," *Nature* 422, no. 6928 (2003): 198–207, https://doi.org/10.1038/nature01511.

13. S. J. Blanksby and T. W. Mitchell, "Advances in Mass Spectrometry for Lipidomics," *Annual Review of Analytical Chemistry* 3, no. 1 (2010): 433–465, https://doi.org/10.1146/annurev.anchem.111808.073705.

14. S. Alseekh, A. Aharoni, Y. Brotman, et al., "Mass Spectrometry-Based Metabolomics: A Guide for Annotation, Quantification and Best Reporting Practices," *Nature Methods* 18, no. 7 (2021): 747–756, https://doi.org/10.1038/s41592-021-01197-1.

15. T. Cajka and O. Fiehn, "Comprehensive Analysis of Lipids in Biological Systems by Liquid Chromatography-Mass Spectrometry," *TrAC, Trends in Analytical Chemistry* 61 (2014): 192–206, https://doi.org/10.1016/j.trac.2014.04.017.

16. C. L. Feider, A. Krieger, R. J. DeHoog, and L. S. Eberlin, "Ambient Ionization Mass Spectrometry: Recent Developments and Applications," *Analytical Chemistry* 91, no. 7 (2019): 4266–4290, https://doi.org/10.1021/acs.analchem.9b00807.

17. Z. Takáts, J. M. Wiseman, B. Gologan, and R. G. Cooks, "Mass Spectrometry Sampling Under Ambient Conditions With Desorption Electrospray Ionization," *Science* 306, no. 5695 (2004): 471–473, https://doi.org/10.1126/science.1104404.

18. A. Rossi, L. Castrati, P. Colombo, et al., "Development and Validation of a DESI-HRMS/MS Method for the Fast Profiling of Esomeprazole and Its Metabolites in Rat Plasma: A Pharmacokinetic Study," *Drug Testing and Analysis* 8, no. 2 (2015): 208–213, https://doi.org/10.1002/dta.1805.

19. J. Balog, L. Sasi-Szabó, J. Kinross, et al., "Intraoperative Tissue Identification Using Rapid Evaporative Ionization Mass Spectrometry," *Science Translational Medicine* 5, no. 194 (2013): 194ra93, https://doi.org/10.1126/scitranslmed.3005623.

20. K.-C. Schäfer, T. Szaniszló, S. Günther, et al., "In Situ, Real-Time Identification of Biological Tissues by Ultraviolet and Infrared Laser Desorption Ionization Mass Spectrometry," *Analytical Chemistry* 83, no. 5 (2011): 1632–1640, https://doi.org/10.1021/ac102613m.

21. A. Molnár, G. S. Horkovics-Kováts, N. Kucsma, et al., "Characterisation of Canine and Feline Breast Tumours, Their Metastases, and Corresponding Primary Cell Lines Using LA-REIMS and DESI-MS Imaging," *International Journal of Molecular Sciences* 25, no. 14 (2024): 7752, https://doi.org/10.3390/ijms25147752.

22. M. Paraskevaidi, S. J. S. Cameron, E. Whelan, et al., "Laser-Assisted Rapid Evaporative Ionisation Mass Spectrometry (LA-REIMS) as a Metabolomics Platform in Cervical Cancer Screening," *eBioMedicine* 60 (2020): 103017, https://doi.org/10.1016/j.ebiom.2020.103017.

23. V. Plekhova, L. Van Meulebroek, M. De Graeve, et al., "Rapid Ex Vivo Molecular Fingerprinting of Biofluids Using Laser-Assisted Rapid Evaporative Ionization Mass Spectrometry," *Nature Protocols* 16, no. 9 (2021): 4327–4354, https://doi.org/10.1038/s41596-021-00580-8.

24. C. Cafarella, D. Mangraviti, F. Rigano, P. Dugo, and L. Mondello, "Rapid Evaporative Ionization Mass Spectrometry: A Survey Through 15 Years of Applications," *Journal of Separation Science* 47, no. (9–10) (2024): e2400155, https://doi.org/10.1002/jssc.202400155.

25. K. Wijnant, L. Van Meulebroek, B. Pomian, et al., "Validated Ultra-High-Performance Liquid Chromatography Hybrid High-Resolution Mass Spectrometry and Laser-Assisted Rapid Evaporative Ionization Mass Spectrometry for Salivary Metabolomics," *Analytical Chemistry* 92, no. 7 (2020): 5116–5124, https://doi.org/10.1021/acs.analchem.9b05598.

26. S. J. S. Cameron, A. Perdones-Montero, L. Van Meulebroek, et al., "Sample Preparation Free Mass Spectrometry Using Laser-Assisted Rapid Evaporative Ionization Mass Spectrometry: Applications to Microbiology, Metabolic Biofluid Phenotyping, and Food Authenticity," *Journal of the American Society for Mass Spectrometry* 32, no. 6 (2021): 1393–1401, https://doi.org/10.1021/jasms.0c00452.

27. S. J. S. Cameron, Z. Bodai, B. Temelkuran, et al., "Utilisation of Ambient Laser Desorption Ionisation Mass Spectrometry (ALDI-MS) Improves Lipid-Based Microbial Species Level Identification," *Scientific Reports* 9, no. 1 (2019): 3006, https://doi.org/10.1038/s41598-019-39815-w.

28. V. G. K. Cardoso, J. Balog, G. P. Sabin, and L. W. Hantao, "Sensory Classification of Brazilian Coffea Arabica by Laser-Assisted Rapid Evaporative Ionization Mass Spectrometry and Machine Learning Algorithms," *ACS Omega* 10, no. 18 (2025): 18775–18783, https://doi.org/10.1021/acsomega.5c00404.

29. G. S. Horkovics-Kováts, D. Simon, R. Schäffer, et al., "Characterization of Blood Serum and Cell Lines by an Automated High-Throughput Well Plate Sampling System Using Laser Ablation-Rapid Evaporative Ionization Mass Spectrometry," *Analytical and Bioanalytical Chemistry* 418, no. 12 (2026): 3773–3789, https://doi.org/10.1007/s00216-026-06484-4.

30. E. A. Jones, D. Simon, T. Karancsi, J. Balog, S. D. Pringle, and Z. Takats, "Matrix Assisted Rapid Evaporative Ionization Mass Spectrometry," *Analytical Chemistry* 91, no. 15 (2019): 9784–9791, https://doi.org/10.1021/acs.analchem.9b01441.

31. M. J. Conroy, R. M. Andrews, S. Andrews, et al., "LIPID MAPS: Update to Databases and Tools for the Lipidomics Community," *Nucleic Acids Research* 52, no. D1 (2023): D1677–D1682, https://doi.org/10.1093/nar/gkad896.

32. D. Božič, D. Vozel, M. Hočevar, et al., "Enrichment of Plasma in Platelets and Extracellular Vesicles by the Counterflow to Erythrocyte Settling," *Platelets* 33, no. 4 (2022): 592–602, https://doi.org/10.1080/09537104.2021.1961716.

10969888c, 2026, 8, Downloaded from https://analyticalsciencejournals.onlinelibrary.wiley.com/doi/10.1002/jms.70077 by Cochrane Slovenia, Wiley Online Library on [10/11/2026]. See the Terms and Conditions (https://onlinelibrary.wiley.com/terms-and-conditions) on Wiley Online Library for rules of use; OA articles are governed by the applicable Creative Commons License

33. J. N. Van Der Veen, J. P. Kennelly, S. Wan, J. E. Vance, D. E. Vance, and R. L. Jacobs, "The Critical Role of Phosphatidylcholine and Phosphatidylethanolamine Metabolism in Health and Disease," *Biochimica et Biophysica Acta, Biomembranes* 1859, no. 9 (2017): 1558–1572, https://doi.org/10.1016/j.bbamem.2017.04.006.

34. Z. Wang, E. Klipfell, B. J. Bennett, et al., "Gut Flora Metabolism of Phosphatidylcholine Promotes Cardiovascular Disease," *Nature* 472, no. 7341 (2011): 57–63, https://doi.org/10.1038/nature09922.

35. W. H. W. Tang, Z. Wang, B. S. Levison, et al., "Intestinal Microbial Metabolism of Phosphatidylcholine and Cardiovascular Risk," *New England Journal of Medicine* 368, no. 17 (2013): 1575–1584, https://doi.org/10.1056/nejmoa1109400.

36. L. Whiley, A. Sen, J. Heaton, et al., "Evidence of Altered Phosphatidylcholine Metabolism in Alzheimer's Disease," *Neurobiology of Aging* 35, no. 2 (2013): 271–278, https://doi.org/10.1016/j.neurobiolaging.2013.08.001.

37. J. M. Vukajlović, D. Drakulić, S. Pejić, et al., "Increased Plasma Phosphatidylcholine/Lysophosphatidylcholine Ratios in Patients With Parkinson's Disease," *Rapid Communications in Mass Spectrometry* 34, no. 4 (2020): e8595, https://doi.org/10.1002/rcm.8595.

38. R. De Freitas Saito, L. N. De Sousa Andrade, S. O. Bustos, and R. Chammas, "Phosphatidylcholine-Derived Lipid Mediators: The Crosstalk Between Cancer Cells and Immune Cells," *Frontiers in Immunology* 13 (2022): 768606, https://doi.org/10.3389/fimmu.2022.768606.

39. M. Hermansson, K. Hokynar, and P. Somerharju, "Mechanisms of Glycerophospholipid Homeostasis in Mammalian Cells," *Progress in Lipid Research* 50, no. 3 (2011): 240–257, https://doi.org/10.1016/j.plipres.2011.02.004.

40. M. He, S. Guo, and Z. Li, "In Situ Characterizing Membrane Lipid Phenotype of Breast Cancer Cells Using Mass Spectrometry Profiling," *Scientific Reports* 5, no. 1 (2015): 11298, https://doi.org/10.1038/srep11298.

41. D. Wolrab, R. Jirásko, O. Peterka, et al., "Plasma Lipidomic Profiles of Kidney, Breast and Prostate Cancer Patients Differ From Healthy Controls," *Scientific Reports* 11, no. 1 (2021): 20322, https://doi.org/10.1038/s41598-021-99586-1.

42. S. Ntshangase, S. Khan, L. Bezuidenhout, et al., "Spatial Lipidomic Profiles of Atherosclerotic Plaques: A Mass Spectrometry Imaging Study," *Talanta* 282 (2024): 126954, https://doi.org/10.1016/j.talanta.2024.126954.

43. T. L. Toft-Bertelsen, S. N. Andreassen, A. H. Simonsen, S. G. Hasselbalch, and N. MacAulay, "The CSF Lipid Profile in Patients With Probable Idiopathic Normal Pressure Hydrocephalus Differs From Control but Does Not Differ Between Shunt Responders and Non-Responders," *Brain Communications* 6, no. 6 (2024): fcae388, https://doi.org/10.1093/braincomms/fcae388.

44. Y. Liu, A. Thalamuthu, K. A. Mather, et al., "Plasma Lipidome Is Dysregulated in Alzheimer's Disease and Is Associated With Disease Risk Genes," *Translational Psychiatry* 11, no. 1 (2021): 344, https://doi.org/10.1038/s41398-021-01362-2.

45. O. Quehenberger and E. A. Dennis, "The Human Plasma Lipidome," *New England Journal of Medicine* 365, no. 19 (2011): 1812–1823, https://doi.org/10.1056/nejmra1104901.

46. D. Božič, M. Hočevar, V. Kononenko, et al., "Pursuing Mechanisms of Extracellular Vesicle Formation," in *Effects of Sample Processing. Advances in Biomembranes and Lipid Self-Assembly* (Academic Press, 2020), 113–155, https://doi.org/10.1016/bs.abl.2020.09.003.

47. V. Šuštar, A. Bedina Zavec, R. Štukelj, et al., "Nanoparticles Isolated From Blood: A Reflection of Vesiculability of Blood Cells During the Isolation Process," *International Journal of Nanomedicine* (2011): 2737–2748, https://doi.org/10.2147/ijn.s24537.

48. R. Nieuwland and P. R. Siljander, "A Beginner's Guide to Study Extracellular Vesicles in Human Blood Plasma and Serum," *Journal of Extracellular Vesicles* 13, no. 1 (2024): e12400, https://doi.org/10.1002/jev2.12400.

49. B. W. Sódar, Á. Kittel, K. Pálóczi, et al., "Low-Density Lipoprotein Mimics Blood Plasma-Derived Exosomes and Microvesicles During Isolation and Detection," *Scientific Reports* 6, no. 1 (2016): 24316, https://doi.org/10.1038/srep24316.

50. E. Á. Tóth, L. Turiák, T. Visnovitz, et al., "Formation of a Protein Corona on the Surface of Extracellular Vesicles in Blood Plasma," *Journal of Extracellular Vesicles* 10, no. 11 (2021): e12140, https://doi.org/10.1002/jev2.12140.

51. J. B. German, J. T. Smilowitz, and A. M. Zivkovic, "Lipoproteins: When Size Really Matters," *Current Opinion in Colloid & Interface Science* 11, no. 2–3 (2006): 171–183, https://doi.org/10.1016/j.cocis.2005.11.006.

52. S. Mora, J. D. Otvos, N. Rifai, R. S. Rosenson, J. E. Buring, and P. M. Ridker, "Lipoprotein Particle Profiles by Nuclear Magnetic Resonance Compared With Standard Lipids and Apolipoproteins in Predicting Incident Cardiovascular Disease in Women," *Circulation* 119, no. 7 (2009): 931–939, https://doi.org/10.1161/circulationaha.108.816181.

53. E. I. Buzás, E. Á. Tóth, B. W. Sódar, and K. É. Szabó-Taylor, "Molecular Interactions at the Surface of Extracellular Vesicles," *Seminars in Immunopathology* 40, no. 5 (2018): 453–464, https://doi.org/10.1007/s00281-018-0682-0.

54. B. György, K. Módos, É. Pállinger, et al., "Detection and Isolation of Cell-Derived Microparticles Are Compromised by Protein Complexes Resulting From Shared Biophysical Parameters," *Blood* 117, no. 4 (2011): e39–e48, https://doi.org/10.1182/blood-2010-09-307595.

55. L. Zhang, J. Song, G. Cavigiolio, et al., "Morphology and Structure of Lipoproteins Revealed by an Optimized Negative-Staining Protocol of Electron Microscopy," *Journal of Lipid Research* 52, no. 1 (2011): 175–184, https://doi.org/10.1194/jlr.d010959.

Supporting Information

Additional supporting information can be found online in the Supporting Information section. **Figure S1:** MS/MS spectrum of *m/z* 742.539 corresponding to PE(36:2) and PC(34:2). **Figure S2:** MS/MS spectrum of m/z 770.571 corresponding to PC(36:2). **Figure S3:** MS/MS spectrum of m/z 818.547 corresponding to PC(36:3). **Figure S4:** MS/MS spectrum (at lower collision energy) of m/z 820.563 corresponding to PC(36:2). **Figure S5:** MS/MS spectrum (at higher collision energy) of m/z 820.563 corresponding to PC(36:2). **Figure S6:** Representative mass spectra of equine plasma samples stored at three different temperatures (4°C, −20°C, −80°C), following optimal sample preparation conditions (centrifugation for 5 min at 80 × g). Spectra were acquired by LA-REIMS and represent the average of five scans. The 600–900 m/z region displays distinct lipidomic profiles, whereas the lower m/z region contains abundant metabolic signals. Samples stored at 4°C exhibited markedly higher signal intensities in the metabolic region, in some cases exceeding those of the lipidomic region. This suggests potential degradation or altered metabolite release due to suboptimal storage conditions. **Table S1:** Statistical parameters—mean, standard deviation, RSD% and standard error—of lipid relative intensities for each centrifugation condition in equine plasma for the m/z 820.563 peak corresponding to PC(36:2).

10969888c, 2026, 8, Downloaded from https://analyticalsciencejournals.onlinelibrary.wiley.com/doi/10.1002/jms.70077 by Cochrane Slovenia, Wiley Online Library on [10/11/2026]. See the Terms and Conditions (https://onlinelibrary.wiley.com/terms-and-conditions) on Wiley Online Library for rules of use; OA articles are governed by the applicable Creative Commons License